Molecular Cell 22, 451–462, May 19, 2006 ©2006 Elsevier Inc. DOI 10.1016/j.molcel.2006.03.036

Central Pore Residues Mediate the p97/VCP Activity Required for ERAD

Byron DeLaBarre,[1,2,3,4,6,7] John C. Christianson,[5,6,7] Ron R. Kopito,[5,6] and Axel T. Brunger[1,2,3,4,6,*]
[1] Howard Hughes Medical Institute
[2] Department of Molecular and Cellular Physiology
[3] Department of Neurology and Neurological Sciences
[4] Stanford Synchrotron Radiation Laboratory
[5] Department of Biological Sciences
[6] Bio-X Program
Stanford University
J.H. Clark Center E300-C
318 Campus Drive
Stanford, California 94305

Summary

The AAA-ATPase p97/VCP facilitates protein dislocation during endoplasmic reticulum-associated degradation (ERAD). To understand how p97/VCP accomplishes dislocation, a series of point mutants was made to disrupt distinguishing structural features of its central pore. Mutants were evaluated in vitro for ATPase activity in the presence and absence of synaptotagmin I (SytI) and in vivo for ability to process the ERAD substrate TCRα. Synaptotagmin induces a 4-fold increase in the ATPase activity of wild-type p97/VCP (p97/VCP^{wt}), but not in mutants that showed an ERAD impairment. Mass spectrometry of crosslinked synaptotagmin · p97/VCP revealed interactions near Trp551 and Phe552. Additionally, His317, Arg586, and Arg599 were found to be essential for substrate interaction and ERAD. Except His317, which serves as an interaction nexus, these residues all lie on prominent loops within the D2 pore. These data support a model of substrate dislocation facilitated by interactions with p97/VCP's D2 pore.

Introduction

p97/VCP is a mammalian ortholog of a eukaryotic protein conserved among flies (Pinter et al., 1998), yeast (Frohlich et al., 1991), plants (Feiler et al., 1995), and protozoans (Roggy and Bangs, 1999). In both mammals and yeast, p97/VCP activity is required to dislocate proteins from the endoplasmic reticulum (ER) to the cytosol during endoplasmic reticulum-associated degradation (ERAD) (Jarosch et al., 2002; Rabinovich et al., 2002; Ye et al., 2001). Dislocation is essential because degradation occurs by the cytosolic ubiquitin-proteasome system (UPS) and not in the ER lumen (Kopito, 1997). Unchecked accumulation of misfolded proteins in the ER induces the unfolded protein response (Kozutsumi et al., 1988) and can result in cell death.

Structurally, p97/VCP is comprised of six identical ~90 kDa protomers. Each protomer has three domains joined by short, well-conserved linkers. The N-terminal domain is followed by tandem repeats (D1, D2) of an AAA domain (ATPases associated with a variety of cellular activities) (Beyer, 1997; Neuwald et al., 1999). N-terminal domains are necessary for interaction of p97/VCP with its adaptor proteins (Meyer et al., 2000; Ye et al., 2001; Zhong et al., 2004) and ER membrane receptors (Lilley and Ploegh, 2004; Ye et al., 2004; Zhong et al., 2004). The D1 and D2 AAA domains are comprised of elements necessary to catalyze ATP hydrolysis and to communicate the nucleotide state throughout the molecule. Both X-ray crystallography (DeLaBarre and Brunger, 2005; Huyton et al., 2003) and solution X-ray scattering (Davies et al., 2005) studies indicate that p97/VCP flips between two major conformations during the ATP hydrolysis cycle. These conformations are referred to as the preactivated (apo and ATP) and activated ($ATP^{\ddagger}$ and ADP) states (DeLaBarre and Brunger, 2005).

The six p97/VCP protomers form a 70 Å-long pore coincident with the six-fold axis of the hexamer (Figure 1A). At the D2 end of p97/VCP, there are two conspicuous loops lining the pore. The first loop contains two strictly conserved arginines, Arg586 and Arg599 (Figure 1B, panel I). These two residues form a double ring near the entrance to the pore at the D2 end of p97/VCP. The second loop includes two conserved hydrophobic residues, Trp551 and Phe552, that are located close to the interface between the D1 and D2 domains (Figure 1B, panel II). These residues are analogous to hydrophobic pore residues that interact with substrate in the Hsp/Clp heat shock proteins (Lum et al., 2004; Weibezahn et al., 2004). Both loops exhibit conformational changes coupled to the switch between the preactivated and activated states of p97/VCP (DeLaBarre and Brunger, 2003, 2005).

ATP hydrolysis by p97/VCP is required for protein dislocation during ERAD (Ye et al., 2001). Members of the AAA family use the ATP hydrolysis cycle to produce conformational changes in their substrate molecules (DeLaBarre and Brunger, 2005; Lupas and Martin, 2002; Neuwald et al., 1999). Some AAA proteins can thread substrate through their central pore (Sousa et al., 2000; Weibezahn et al., 2004). A similar mechanism has been proposed for p97/VCP based on low-resolution electron microscopy studies of isolated p97/VCP (Beuron et al., 2003), although more recent biochemical and structural data have cast doubts on this model (Davies et al., 2005; DeLaBarre and Brunger, 2003; Song et al., 2003). Up to now, lack of a physiological substrate for in vitro studies of substrate · p97/VCP interactions has limited the functional understanding of p97/VCP. The mechanism of action for p97/VCP has yet to be elucidated.

Here, we have probed the importance of selected residues throughout the central pore of p97/VCP for ATPase activity, substrate interactions, and ERAD activity (Figure 1). Point mutants of *Mus musculus* p97/VCP were characterized in vitro with a steady-state analysis of ATPase activity in the presence and absence of a physiological substrate. We found that synaptotagmin I (SytI) accelerates ATPase activity of wild-type p97/VCP (p97/VCP^{wt}), but not that of p97/VCP mutants that reduce or

*Correspondence: brunger@stanford.edu
[7] These authors contributed equally to this work.

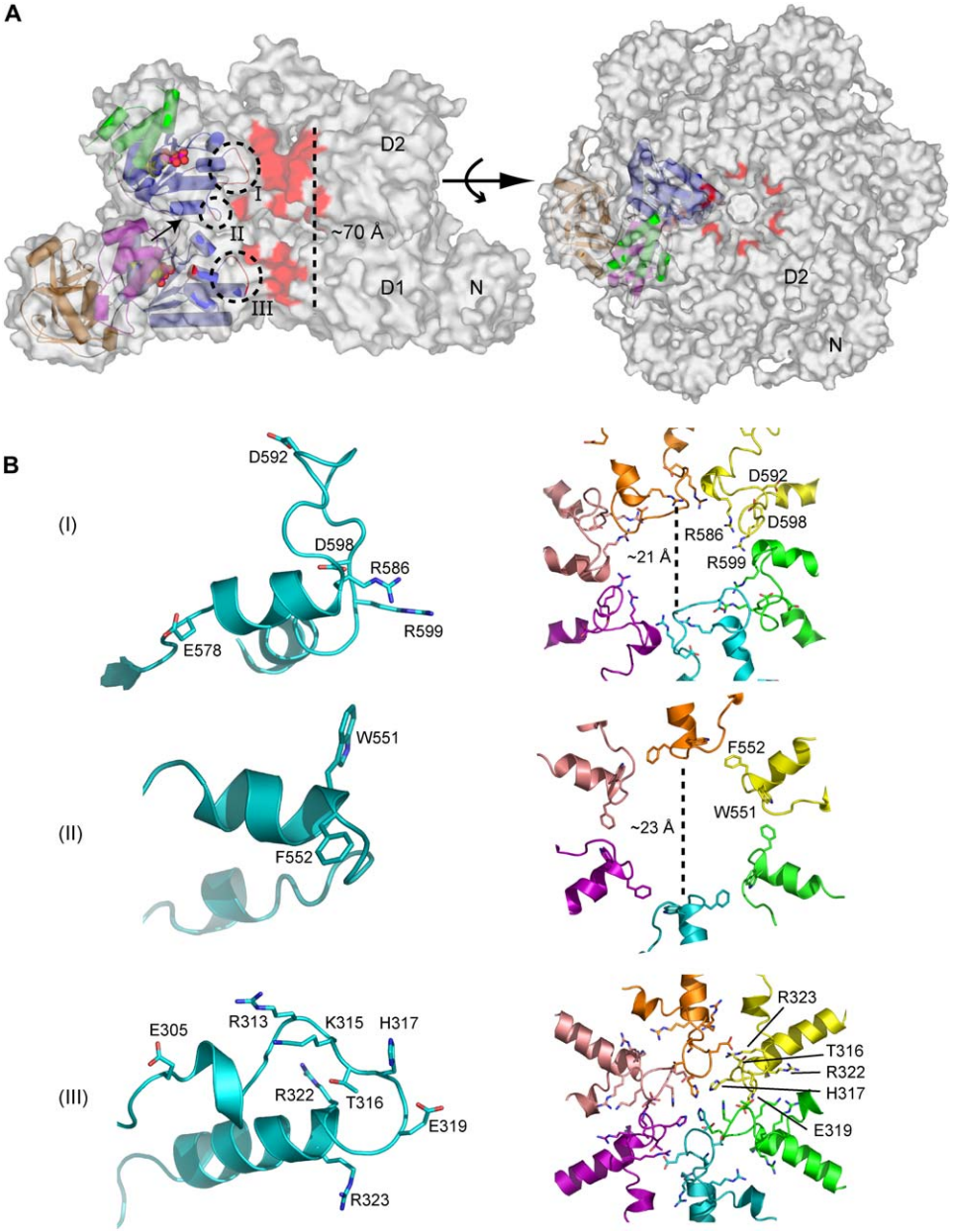

Figure 1. Location of Mutated Residues Lining the Pore of p97/VCP

(A) The p97/VCP · ADP hexamer is shown in a space-filling view with one of the protomers shown as cartoon (nucleotide as spheres). A side-on view (left panel) is shown with two of the protomer subunits cut away to reveal the central pore. The protomer is colored as follows: N domain, brown; D1 and D2 α/β, blue; D1α, purple; D2α, green. All of the Walker A/B and the SRH residues are near the nucleotide and not near the pore. Loops are highlighted by circles, (I) Arg586/Arg599, (II) Trp551/Phe552, and (III) His317 loop, and are colored red in the space-filling view. The arrow near loop (II) indicates the p97/VCP · Sytl crosslinked region. The right panel shows a view looking down from the D2 end of the molecule. The location of the Arg586/Arg599 pair is colored red, and a cartoon protomer is given for reference.

(B) Detailed views of the pore loops shown both for the protomer (left panels) and the molecular hexamer (right panels). In the hexamer views, protomers are uniquely colored and one of the protomers labeled.

eliminate the basal ATPase activity. Sytl is the first protein observed to accelerate p97/VCP ATPase activity. We further characterized the interaction between Sytl and p97/VCP^{wt} by mass spectrometry. p97/VCP mutants were also studied in vivo using a cell-based assay that monitors degradation of the ERAD target TCRα. Collectively, our findings indicate that substrate interactions occur at the D2 end of p97/VCP.

Results

Rationale of Point Mutation Selection

To investigate the functional importance of distinct structural features within p97/VCP, we employed site-directed mutagenesis. One class of mutations was in the SRH domain, a defining feature of the AAA proteins proposed to play a role in interprotomer communication (Neuwald

et al., 1999; Ogura et al., 2004). We chose residues Arg362 and Arg638 to probe the effect of the SRH on p97/VCP ATPase activity and ERAD. As negative controls for some experiments, mutations in the Walker A/B motifs known to disrupt ATPase activity (Lys251, Glu305, Lys524, Glu578) were also included (Ye et al., 2001).

The second class of mutations consisted of selected residues lining the pore of p97/VCP (Arg313, Lys315, Thr316, His317, Glu319, Trp551, Phe552, Arg586, Asp592, Asp598, Arg599) (Figure 1). The conserved Arg586 and Arg599 residues were chosen because of their prominent location within the D2 pore (Figure 1B, panel I) and their homology to certain arginines in proteasomal Rpt proteins (see Figure S1B in the Supplemental Data available with this article online). We also mutated Asp592 and Asp598 in this region. Residues Trp551 and Phe552 were chosen since they define a conserved hydrophobic ring in the D2 pore (Figure 1B, panel II). Residues 313–323 comprise the loop that defines the narrow constriction of the D1 pore, including His317 (Figure 1B, panel III, and Figure S1A). As negative controls, mutations of Arg322, Arg323, and Arg700 were also included in some experiments.

All mutations except p97/VCP^{K251A} resulted in properly folded and hexameric protein (data not shown). The p97/VCP^{K251A} mutant yielded two pools of full-length p97/VCP, only one of which was hexameric. There was no observable equilibrium between the hexameric and nonhexameric pools of p97/VCP^{K251A}, so the hexameric pool was used for all studies. Previously, the nucleotide in the D1 domain was shown to stabilize the hexamer (Wang et al., 2003). Since Lys251 interacts directly with the D1 bound ADP molecule (DeLaBarre and Brunger, 2005), the reduced stability of the hexamer is not surprising.

ATPase Steady-State Kinetics

Steady-state kinetic analyses were carried out for all p97/VCP mutants except some of those that showed insignificant reduction of ERAD activity in vivo (Table 1). We first examined the basal ATPase activity of p97/VCP by carrying out the ATPase analyses in the absence of protein substrate. Progress curves from the p97/VCP^{wt} and most mutants could be interpreted with a simple Michaelis-Menten kinetic model (Figure 2, Figure S2, Table 1). The wild-type kinetic parameters we obtained compare well with those measured in previous studies (Meyer et al., 1998; Song et al., 2003; Zalk and Shoshan-Barmatz, 2003).

The Walker A/B mutants p97/VCP^{K251A} and p97/VCP^{E578Q} both had activities below the detection limit of our ATPase activity assay. The two other Walker A/B mutants, p97/VCP^{E305Q} and p97/VCP^{K524A}, produced measurable k_{cat} and K_M values; p97/VCP^{E305Q} exhibited an ~2-fold drop in k_{cat}/K_M versus wild-type, and p97/VCP^{K524A} exhibited an ~10-fold drop in k_{cat}/K_M versus wild-type. The slight (~2 fold) drop in K_M for the p97/VCP^{K524A} mutant is surprising, given its proposed role of nucleotide binding. However, K_M is not a direct measure of nucleotide binding affinity, and the larger (~20-fold) drop in k_{cat} for this mutation suggests that this residue is involved in both the binding and hydrolysis of nucleotide. Both the p97/VCP^{E305Q} and p97/VCP^{K524A} mutants also exhibited a decrease in cooperativity (Table 1). The strong effect on kinetic parameters by the Walker A/B mutations is consistent with the known importance of these residues in ATPases. The reduction of ATPase activity by the Walker A/B mutations in the D1 domain presumably arises due to a structural destabilization of the hexamer since the D1 domain has been found to be catalytically inactive (Wang et al., 2003).

SRH arginines reach between protomers to interact with neighboring nucleotides. The SRH mutants, p97/VCP^{R362A} and p97/VCP^{R638A}, showed ~13- and ~100-fold decreases in k_{cat}/K_M, respectively (Table 1 and Figure 2A). The cooperativity of p97/VCP^{R362A} was strongly decreased, whereas that of p97/VCP^{R638A} was essentially wild-type (Table 1 and Figure 2B). The stronger decrease in ATPase activity observed for p97/VCP^{R638A} supports the role of p97/VCP-D2 as the active ATPase domain, but the lack of an effect on cooperativity is surprising. It is therefore possible that the SRH Arg638 in the D2 domain is simply a catalytic residue and does not play a role in interprotomer communication. In support of this, we did not observe direct interactions between the D2 SRH region and the bound nucleotides in the crystal structures (DeLaBarre and Brunger, 2003, 2005).

Of the mutations made to residues lining the pore of p97/VCP, several produced notable changes in steady-state parameters. In the loop defining the narrow constriction of the D1 pore, p97/VCP^{R313A} and p97/VCP^{K315L} showed an ~20- and ~5-fold reduction in k_{cat}/K_M, respectively, with little change in cooperativity. The p97/VCP^{H317A} mutant yielded an ~6-fold reduction in both k_{cat} and K_M (Table 1) with little change in k_{cat}/K_M but exhibited a dramatic switch from positive to negative cooperativity (Figure 2B). Other substitutions in the D1 pore exhibited near-wild-type k_{cat}/K_M values with little change to cooperativity. At the D2 end of the pore, the p97/VCP^{R586A} and p97/VCP^{R599A} mutants both produced substantial decreases (~30-fold) in k_{cat}/K_M when compared to p97/VCP^{wt} (Table 1 and Figure 2A). While all substitutions at these residues showed diminished cooperativity, only p97/VCP^{R586A} exhibited a complete disappearance of cooperative behavior during ATP hydrolysis (Figure 2B). Further inside the D2 pore, both the p97/VCP^{W551A} single mutant and the p97/VCP^{W551AF552A} double mutant showed decreased k_{cat}/K_M, with the latter having a greater reduction. The Hill coefficients were decreased only slightly from wild-type values. Altogether, these data implicate the D1 loop that includes His317 and the pore-lining residues of D2 (Arg586, Arg599, Trp551, and Phe552) as being critical for the proper function of p97/VCP.

SytI Accelerates In Vitro ATPase Activity

During the search for an in vitro substrate of p97/VCP, we discovered that the cytoplasmic fragment (including both the C2A and C2B domains) of SytI accelerates ATPase activity of p97/VCP^{wt} 4-fold (Figure 2C). An interpretation of this acceleration is that SytI is acting as a substrate of p97/VCP. In contrast, the adaptor protein p47 decreases ATPase activity (Meyer et al., 1998). p97/VCP mutants showed differential ATPase acceleration upon addition of the cytoplasmic fragment of SytI (Figure 2C). There was a strong correlation between mutants with impaired basal ATPase activity and those that did not show an acceleration of ATPase activity in

Table 1. Steady-State Enzyme Kinetics

Mutation	k_{cat} (nmol P_i μg protein^{-1} min^{-1})	K_M (μM)	k_{cat}/K_M (nmol P_i μg protein^{-1} min^{-1} μM ATP)	n	Normalized Fluoresecence from Cell-Based Assay
Wild-type	0.57(1)	49(2)	$1.2(1) \times 10^{-2}$	1.5(1)	1.0 (1)
Walker A/B					
K251A	< .001[a]	> 215[a]	—	—	3.7(2)
E305Q	0.27(2)	53(11)	$5(1) \times 10^{-3}$	1.1(1)	3.4(1)
K524A	.024(3)	18(5)	$1.3(5) \times 10^{-3}$	0.7(1)	3.6(1)
E578Q	< .001[a]	> 215[a]	—	—	2.86(8)
SRH					
R362A	0.027(1)	31(2)	$9.0(6) \times 10^{-4}$	1.1(1)	1.50(2)
R638A	0.004(1)	31(2)	$1.2(1) \times 10^{-4}$	1.4(1)	2.47(1)
D1 Pore					
R313A	0.020(1)	33(1)	$6.0(4) \times 10^{-4}$	1.3(1)	1.5(1)
R313K	0.054(1)	21(1)	$3.0(2) \times 10^{-3}$	1.2(1)	1.09(6)
K315L	0.120(4)	79(8)	$1.5(2) \times 10^{-3}$	1.3(1)	1.15(1)
T316V	0.43(1)	75(4)	$5.7(5) \times 10^{-3}$	1.7(1)	1.12(1)
H317Q	0.73(1)	83(3)	$8.8(5) \times 10^{-3}$	1.5(1)	1.02(1)
H317N	0.436(6)	49(2)	$9.0(5) \times 10^{-3}$	1.5(1)	1.09(1)
H317A	0.09(1)	7(1)	$1.2(3) \times 10^{-2}$	0.8(1)	3.36(4)
E319L	0.56(1)	71(3)	$7.9(5) \times 10^{-3}$	1.4(1)	1.40(1)
E319Q	0.85(2)	48(3)	$1.8(2) \times 10^{-2}$	1.5(1)	1.32(1)
R322A	—	—	—	—	1.25(1)
R322K	—	—	—	—	1.1(1)
R323A	—	—	—	—	1.30(1)
R323K	—	—	—	—	1.15(1)
D2 Pore					
W551A	0.022(1)	3(1)	$7.0(4) \times 10^{-3}$	1.2(2)	2.42(3)
F552A	—	—	—	—	1.50(5)
W551AF552A	0.023(1)	15(3)	$1.5(3) \times 10^{-3}$	1.2(2)	3.2(1)
R586A	0.004(1)	14(1)	$3.2(2) \times 10^{-4}$	1.0(1)	3.3(2)
R586K	0.007(1)	14(1)	$6.8(4) \times 10^{-4}$	1.2(1)	2.16(2)
D592N	—	—	–	—	1.18(1)
D598N	—	—	—	—	0.96(6)
R599A	0.005(1)	14(1)	$3.8(3) \times 10^{-4}$	1.2(1)	2.82(5)
R599K	~0.001[a]	~13[a]	$\sim 3 \times 10^{-4}$	—	1.71(4)
In Vivo Controls					
CTRL shRNA	—	—	—	—	1.00(4)
VCP/p97 shRNA	—	—	—	—	2.84(3)
MG-132					11.9(9)

Number in parenthesis is the absolute error in the final digit of the reported value.
[a] These mutants exhibited minimal activity and produced ATP progress curves that could not be fit with Michaelis-Menten kinetics. Best estimates of these values are reported.

the presence of the cytoplasmic fragment of SytI. The two exceptions to this correlation are the p97/VCP^{H317N} and p97/VCP^{W551A} mutants (discussed below).

Interaction between SytI and p97/VCP

An interaction between p97/VCP and the C2A domain of SytI was previously reported (Miller, 1993; Sugita and Südhof, 2000) but dismissed as nonphysiological because the role of p97/VCP was at the time believed to be in synaptic vesicle fusion rather than ERAD, and p97/VCP is found in all tissues, whereas SytI is specific to brain tissue. Because SytI has an N-terminal transmembrane helix and a glycosylated luminal domain (Han et al., 2004), it likely passes through an ERAD checkpoint during its maturation, thereby coming into contact with p97/VCP. Indeed, a small fraction of SytI is localized in the ER and accumulates as a ubiquitylated form in the presence of proteasome inhibitor (Figure 3A).

We established an in vitro interaction between the cytoplasmic fragment of SytI and p97/VCP by observing a native gel mobility shift when SytI is in molar excess of the p97/VCP hexamer (Figure 3B). This effect was somewhat decreased when the p97/VCP^{W551A} and p97/VCP^{W551AF552A} mutants were used. A similar decrease in binding affinity was observed with pull-down experiments using GST-tagged SytI (data not shown). We observed direct crosslinking between certain lysines of the two proteins and identified the interacting regions by mass spectrometry using a mixture of crosslinker isotopes (Figures 3C and 3D). The particular interaction occurs between p97/VCP^{K565} and either SytI^{K236} or SytI^{K244} (Figures 1A, 3D, and 3E).

Monitoring p97/VCP Activity in ERAD

To investigate the functional consequences of mutations in p97/VCP, we developed a cell-based assay to evaluate the integrity of ERAD in vivo. SytI was not

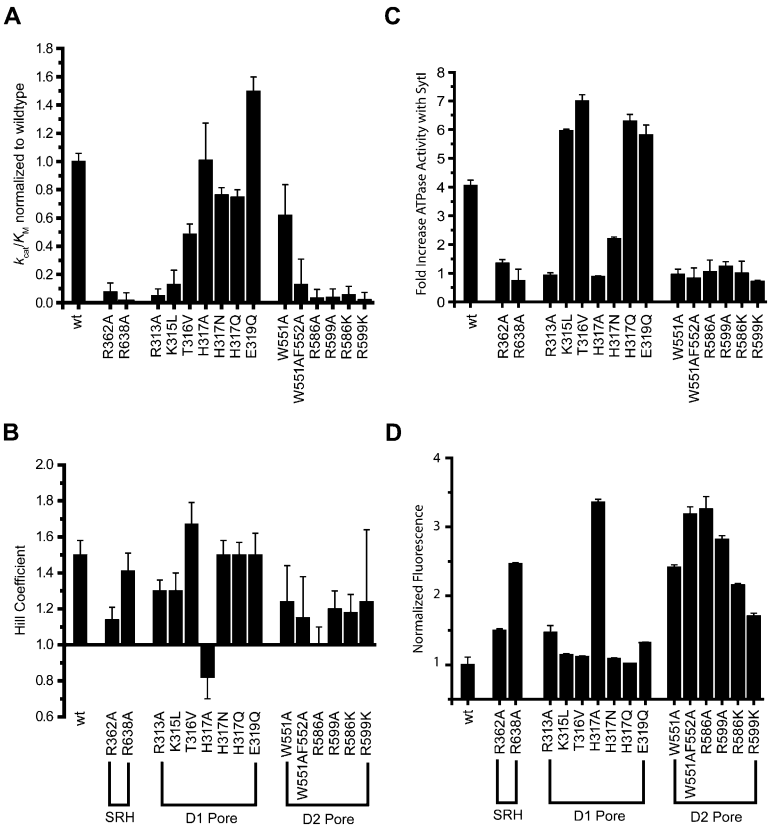

Figure 2. ATPase and Functional Assays of p97/VCP Mutants

(A) k_{cat}/K_M for selected mutants. Values have been normalized to that of the wild-type protein. Errors are derived from curve fitting.

(B) Hill coefficient, n, for selected mutants. Note that the abscissa has been offset by +1 in this plot to demarcate the difference between positive cooperativity, noncooperativity, and anticooperativity. The Hill coefficient was determined from progress curve fitting parameters.

(C) Fold increase in ATPase activity for p97/VCP^{wt} and mutants in the presence of the excess cytoplasmic fragment of SytI. The experiment was performed with 215 μM ATP, a saturating ATP condition as determined from p97/VCP^{wt} in the absence of substrate.

(D) Summary of effects on TCRα-GFP degradation in reporter cells transfected with p97/VCP mutants. Data were normalized to p97/VCP^{wt} and shown as the fold increase in mean fluorescence. For (C) and (D), mean and standard deviation values from multiple experiments are shown.

practical for these studies since the majority matures properly and avoids ERAD, thereby obscuring measurable signal with background noise levels. We therefore employed TCRα, a well-characterized ERAD substrate (Huppa and Ploegh, 1997; Tiwari and Weissman, 2001; Yu et al., 1997; Yu and Kopito, 1999). Using a clonal reporter line that stably expressed a TCRα-GFP fusion protein, impairment of ERAD was reflected simply by accumulation of GFP fluorescence (and hence substrate) as measured by flow cytometry (Figure 4A). A similar reporter system with EGFP-tagged MHC Class I has been used previously to screen for compounds that inhibit substrate dislocation (Fiebiger et al., 2004). Treating TCRα-GFP reporter cells with the proteasome inhibitor MG132 resulted in a mean fluorescence increase of more than 10-fold (Table 1), illustrating the reporter's ability to reflect the integrity of ERAD.

Because the proposed role of p97/VCP in ERAD lies upstream of the proteasome, we reasoned that TCRα-GFP degradation would be disrupted if p97/VCP mutants acted as functional dominant negatives. As mentioned above, all p97/VCP mutants except K251A assembled into functional hexamers in vitro, but to confirm that assembly also occurred in vivo, lysates from cells expressing myc-tagged p97/VCP^{wt} and p97/VCP^{H317A} were separated on sucrose gradients (Figure 4B). Both mutant and p97/VCP^{wt} were found to sediment between 450 and 600 kDa, appropriate for hexameric assembly (~540 kDa). As mutant p97/VCP hexamers are likely to be heteromeric in vivo (with endogenous p97/VCP), dominant-negative effects on ERAD may be attenuated relative to those measured from homomeric mutants in vitro.

Each of the selected p97/VCP mutants was expressed in the TCRα-GFP reporter cell line. To facilitate detection and analysis of only the p97/VCP^{+} cells, a truncated CD4 cell surface marker (ΔCD4) under the control of an IRES element was employed. We undertook a functional evaluation of the effects of the transiently expressed p97/VCP-IRES-ΔCD4 mutants on ERAD by measuring GFP fluorescence change in CD4^{+} (i.e., p97/VCP^{+}) cells (Figure 2D, Figure S3, Table 1). Mean fluorescence values obtained from p97/VCP^{+} cells are a measure of accumulated substrate and thus reflect the relative functional impairment a particular p97/VCP mutant has on ERAD. These values do not reflect any impact an individual p97/VCP mutant may have had on cell survival, as an identical number of CD4^{+} events were evaluated for each mutant (Figures S4 and S5).

Dominant-Negative Impairment of ERAD by p97/VCP Mutants

ERAD impairment resulted from the direct loss of p97/VCP activity due to the assembly of dysfunctional (dominant-negative) hexamers, as confirmed by gene silencing of endogenous p97/VCP with a short-hairpin RNA (shRNA) (Table 1). It is important to note that high expression levels of some p97/VCP mutants (particularly those in the D2 domain) were not well tolerated for these assays, exhibiting lethality in some transfected cells. p97/VCP's yeast ortholog Cdc48p is an essential gene, and so this finding is not unexpected. It suggests that too severe an impairment to p97/VCP function in mammalian cells is lethal, a conclusion that is supported by the observation of a dramatic reduction in the

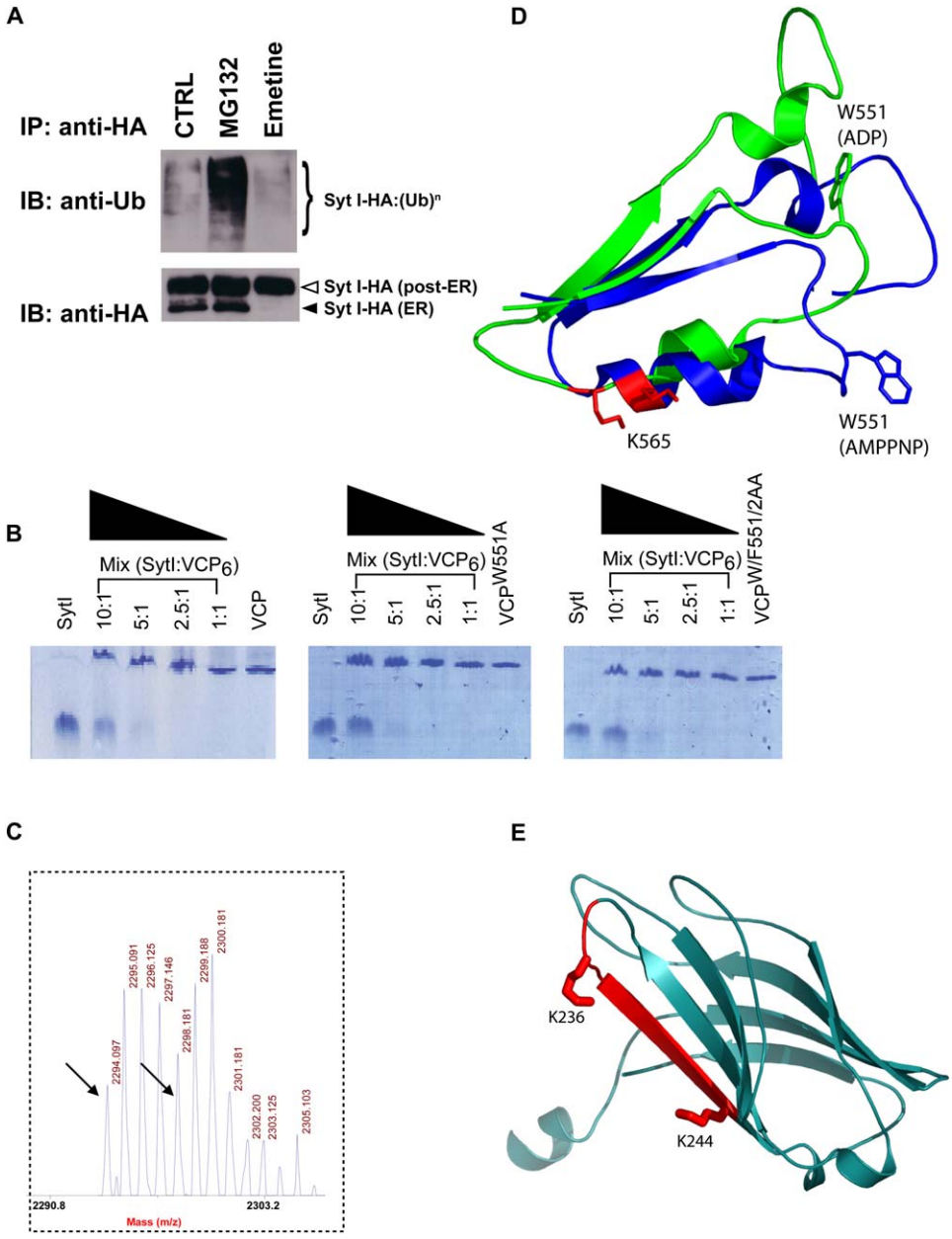

Figure 3. Interaction between p97/VCP and SytI

(A) HEK293 cells expressing SytI-HA were treated with DMSO (CTRL), 10 μM MG132, or 10 μM emetine for 6 hr. SytI-HA was immunoprecipitated (IP) from lysates by anti-HA and immunoblotted (IB) with anti-Ub (top) and anti-HA (bottom). The black arrowhead designates the ER form of SytI-HA, which was confirmed by sensitivity to EndoH treatment and by Concanavilin A affinity purification (data not shown). Inclusion of the translation inhibitor emetine demonstrates that the ER form of SytI-HA is transient.

(B) Native gel shift of p97/VCP, p97/VCP^{W551A}, and p97/VCP^{W551AF552A} by SytI. Coomassie staining was used. The total protein concentration was ~1 mg/ml in each lane. Molar [SytI]:[p97/VCP$_6$] ratios are shown on top. The upward shift of the top band is indicative of complex formation. Note the decreased effect for the mutants versus p97/VCP^{wt}.

(C) Mass spectrum showing crosslinked peptide using a mixture of isotope states. The MH$^+$ and MH$^+$ + 4 peaks are indicated by arrows. The other peaks arise from naturally occurring isotope variance.

(D) Conformational change of residues 537–599, AMP-PNP state (blue), and ADP state (green) (DeLaBarre and Brunger, 2005). This loop moves by ~10 Å between the two nucleotide states such that it is closer to the D2 pore entrance in the ADP state than in the AMP-PNP state. The region identified in the crosslinking experiments is shown in red.

(E) Cartoon rendering of residues 140–265 comprising the C2A domain of SytI (Sutton et al., 1995). The crosslinked peptide is shown in red along with Lys236 and 244, with at least one of them involved in crosslinking.

abundance and expression range of CD4$^+$ cells for some mutants (Figure S5).

Of the mutations in the D1 pore loop (Figure 1B, panel III), only p97/VCP^{H317A} produced an effect on ERAD that was significantly different from that of p97/VCP^{wt} (Figure 2D). Expression of p97/VCP^{H317A} impaired substrate degradation, whereas the in vivo effect of evolutionarily conserved p97/VCP^{H317N} or p97/VCP^{H317Q} mutants

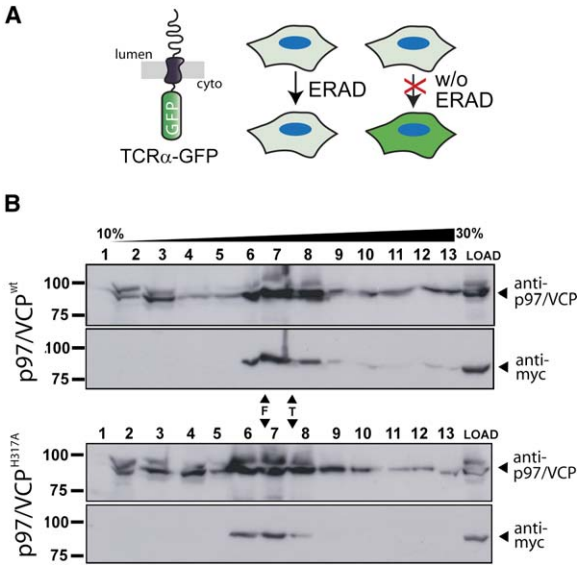

Figure 4. ERAD Assay

(A) Schematic of the ERAD reporter TCRα-GFP (left) and principle behind measuring ERAD by fluorescence change (right).

(B) Velocity sedimentation of transiently expressed p97/VCP-myc on sucrose gradients. Lysates from TCRα-GFP reporter cells transiently expressing myc-tagged p97/VCP^{wt} (top) and p97/VCP^{H317A} (bottom) were separated on 10%–30% sucrose gradients. Western blots of fractions were probed with anti-p97/VCP and anti-myc. F (ferretin, 450 kDa) and T (thyroglobulin, 660 kDa) were run on parallel gradients as molecular weight controls and are indicated by black arrowheads.

was close to that of p97/VCP^{wt} (Figure 2D, Figure S3, Table 1). Mutation of Arg313 had only a slight effect on ERAD, while the remaining residues in the vicinity of His317 had no appreciable effect on ERAD.

TCRα-GFP and p97/VCP^{H317A} colocalized in a perinuclear pattern characteristic of ER (Figure 5A, middle row). This pattern differs from that observed in p97/VCP^{wt} expressing cells exposed to MG132, where TCRα-GFP colocalized with p97/VCP in aggresomes (Figure 5A, bottom row). Expression of either p97/VCP^{H317A} or p97/VCP^{E305Q}, but not p97/VCP^{H317N}, caused TCRα-GFP to accumulate in both full-length and ubiquitylated forms (Figure 5B). Deglycosylated TCRα-GFP was detected in MG132-treated cells expressing p97/VCP^{wt} (see asterisk) but not observed in p97/VCP^{H317A} and p97/VCP^{E305Q} expressing cells. These observations are consistent with the hypothesis that functional p97/VCP is required for dislocation from the ER membrane. It is possible that a small amount of deglycosylated material may be escaping detection, as the amount of TCRα-GFP accumulated with mutant p97/VCP is less than is seen with MG132 treatment. Similar phenotypes were observed for all other mutants that exhibited increased GFP fluorescence.

Of the p97/VCP mutants in the D2 pore, two sets of residues were found to be critical for ERAD. First, the expression of p97/VCP^{R586A} and p97/VCP^{R599A} (Figure 1B, panel I) significantly impaired TCRα-GFP degradation, on par with mutations to the D2 Walker A/B residues (Figure 2D, Table 1). The more conservative arginine to lysine substitutions at the same positions were less severe but still disrupted ERAD. As negative controls, mutations of other exposed D2 loop residues (p97/VCP^{D592N}, p97/VCP^{D598N}) had no significant effect on TCRα-GFP degradation (Table 1), and an arginine to alanine mutant on the exterior of p97/VCP (p97/VCP^{R700A}) was identical to p97/VCP^{wt} (data not shown). Second, mutation of either Trp551 or Phe552 in the hydrophobic pore loop (Figure 1B, panel II) caused ~2- to 3-fold increases in TCRα-GFP fluorescence, with the former being stronger and the double mutant (p97/VCP$^{W551A/F552A}$) having the most substantial effect (Table 1 and Figure 2D). Altogether, these data reaffirm the critical role that p97/VCP plays in ERAD while highlighting the importance pore-lining residues have for p97/VCP function, specifically His317, Trp551, Phe552, Arg586, and Arg599.

Walker A/B mutants (p97/VCP^{K251A}, p97/VCP^{E305Q}, p97/VCP^{K524A}, and p97/VCP^{E578Q}) caused an ~3- to 4-fold increase in mean fluorescence relative to p97/VCP^{wt} (Table 1), confirming that disruption of the nucleotide binding site in either domain affects p97/VCP function in ERAD. Even though p97/VCP^{E305Q} expression impaired ERAD to an extent comparable to that obtained with other Walker mutations, cells appeared to tolerate higher expression levels of this mutant (Figure S5), in agreement with results observed previously (Dalal et al., 2004; Lamb et al., 2001). The SRH mutants exhibited differential effects on TCRα-GFP degradation, with the p97/VCP^{R638A} mutation in D2 causing a greater accumulation of substrate (~2.5-fold) than did the corresponding residue in D1 (p97/VCP^{R362A}, ~1.5-fold). These observations are consistent with the nonequivalence of the D1 and D2 domains, i.e., that the ATPase activity of the D2 domain, but not the D1 domain, is crucial for p97/VCP function (Song et al., 2003).

Correlating ATPase Activity with ERAD

The comparison between in vivo and in vitro studies is not straightforward since the cell-based assay utilizes p97/VCP hexamers that exist as mixtures of wild-type and mutant subunits. Nevertheless, some general observations can be made. Both the in vitro and in vivo analyses presented above demonstrate that some individual residues make substantial contributions to the mechanism of action of p97/VCP. As both coordinated ATP hydrolysis and substrate binding are necessary to dislocate misfolded substrates during ERAD, it is not surprising that all mutants with measurable effects on ERAD exhibited decreased ATPase activity in vitro and/or decreased substrate interaction (Figure 2A).

The high correlation between the ATPase-deficient mutants and the SytI-unaffected mutants is consistent with deficiencies in p97/VCP · SytI interactions or compromised ATPase hydrolysis. The one exception is the p97/VCP^{W551A} mutant (Figures 2A and 2C). This mutant exhibits near-wild-type ATPase activity and kinetic parameters but could not be stimulated by SytI. Furthermore, p97/VCP^{W551A} showed a strong effect on ERAD, suggesting that Trp551 is specifically involved in substrate interaction rather than catalytic activity, which is consistent with our crosslinking data. Generally, mutants that have reduced basal ATPase activity also exhibit reduced ERAD. However, the converse did not always hold true (e.g., p97/VCP^{W551A}). p97/VCP^{H317A} is another example, exhibiting near-wild-type ATPase specific activity due to compensating decreases in both k_{cat} and K_M (Table 1) but impaired ERAD.

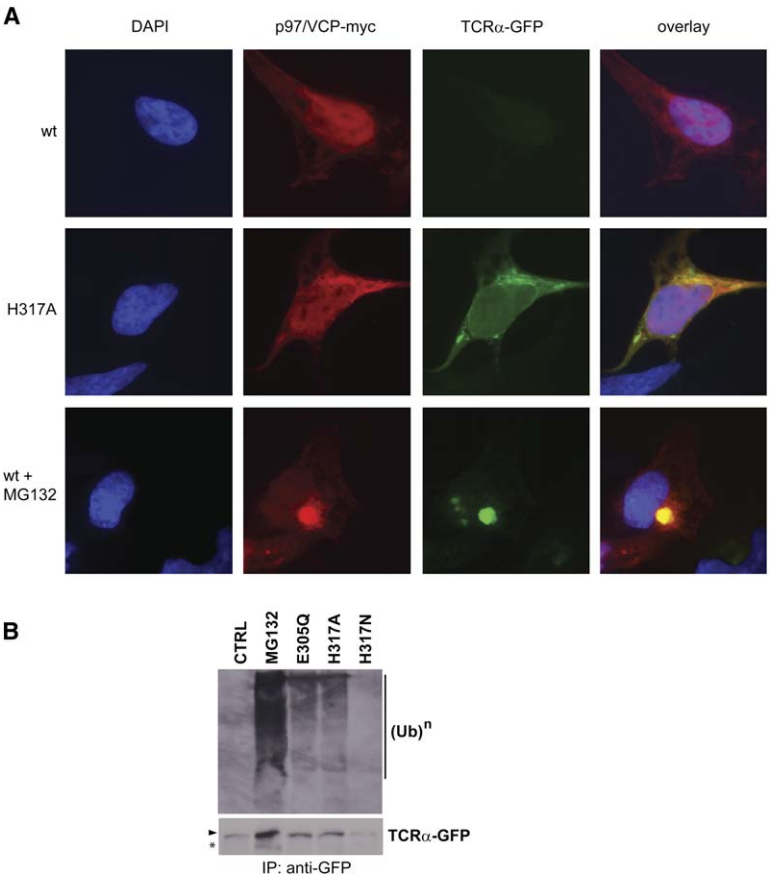

Figure 5. TCRα-GFP Accumulation with p97/VCP Mutants

(A) p97/VCP^{H317A} colocalizes with accumulated TCRα-GFP. TCRα-GFP reporter cells were transfected with p97/VCP^{wt} (top), p97/VCP^{H317A} (middle), or p97/VCP^{wt} + MG132 (bottom). Panels show nuclei (left), TCRα-GFP (middle left), p97/VCP (anti-myc, middle right), and overlay (right).

(B) p97/VCP mutants cause accumulation of TCRα-GFP. TCRα-GFP was immunoprecipitated from lysates of reporter cell transiently expressing p97/VCP^{wt} (± MG132), p97/VCP^{E305Q}, p97/VCP^{H317A}, and p97/VCP^{H317N}. Western blots of immunoprecipitated substrates were probed with anti-ubiquitin (top) and anti-GFP (bottom). An asterisk indicates a lower glycosylation form of TCRα-GFP. p97/VCP^{wt} served as the control.

One additional finding was an apparent inverse correlation between ERAD impairment and cell survival (Figure S5). Given the essential nature of p97/VCP, the observation that mutants causing the greatest impairment of ERAD (e.g., Walker A/B, Arg586, and Arg599) had the most adverse effect on cell survival is not entirely surprising. Interestingly though, as with ATPase activity, p97/VCP^{H317A} was an exception to this correlation indicating that it affects p97/VCP function in a unique manner.

Discussion

D2 Pore Loops Facilitate Substrate Translocation

In the D2 domain of p97/VCP, we focused primarily on two loops in the pore. The first loop, located at the entrance to the D2 end of the pore, contains Arg586 and Arg599 (Figure 1B, panel I). Both arginines are important for ERAD activity and substrate-induced ATPase acceleration (Figures 2C and 2D). Both residues face the central pore in activated (hydrolysis transition and ADP states) conformations but not in the preactivated (ATP and apo states) conformations (DeLaBarre and Brunger, 2005). This switch may be construed as the formation and dissolution of a binding site.

Further supporting evidence for a role of Arg586 and Arg599 in substrate dislocation is that they are strictly conserved between p97/VCP and another group of AAA family members, the proteasomal 19*S* cap ATPases (Rpt proteins, Figure S1B). The strict conservation is underscored by the fact that the six proteasomal ATP-dependent subunits comprising the eukaryotic 19*S* cap are encoded by six different genes. Using an in vitro system, the 19*S* cap of the proteasome was shown to be sufficient to catalyze dislocation of an ERAD target in the absence of Cdc48p (Lee et al., 2004), suggesting that the 19*S* cap and p97/VCP function similarly.

The second loop in the D2 domain contains the conserved Trp551 and Phe552 residues (Figure 1B, panel II). The p97/VCP^{W551A} mutant strongly affected ERAD and substrate-induced ATPase acceleration, but not basal ATPase kinetic parameters (Figure 2). This suggests a role of Trp551 in substrate interaction but not catalytic mechanism. Like the Arg586/Arg599 pair, the Trp551/Phe552 pair is conserved between p97/VCP and the proteasome Rpt proteins, although not as strictly as the arginines discussed above (Figure S1C). The function of the homologous residues in the proteasomal Rpt proteins is unknown, but the similarity is interesting, given the aforementioned comparisons between p97/VCP and the proteasome 19*S* cap. In addition to the sequence conservation with the Rpt proteins, the Trp551/Phe552 pair in p97/VCP is structurally analogous to the hydrophobic GYVG motif found in Hsp/Clp proteins (Lum et al., 2004), for which there is also direct evidence of substrate interaction (Hinnerwisch et al., 2005; Weibezahn et al., 2004). The respective Hsp/Clp and p97/VCP hydrophobic residues are structurally analogous in that they both face into their respective central pores. However, it should be noted that the role of p97/VCP in dislocating protein substrates from the ER is very different from that of the chaperone

function of the Clp proteins. In contrast to Clp proteins, p97/VCP interacts with proteins at the membrane-cytosol interface. The role of p97/VCP and its various adaptor proteins is not to completely unfold and degrade proteins but rather to engage, dislocate, and then hand off ER bound substrates to the 26*S* proteasome. Thus, there is no a priori reason to believe that p97/VCP and Clp proteins have identical mechanisms of action.

The loop bearing Trp551/Phe552 undergoes a large conformational change in the transition from the preactivated to the activated nucleotide states (Figure 3D). The crosslinking data show that SytI interacts with the region just past the Trp551/Phe552 loop (Figures 3C–3E). Taking into account the conformational changes during the ATP hydrolysis cycle observed in X-ray crystal structures and the results of the present study, we propose that the Trp551/Phe552 pair creates a hydrophobic patch for substrate interactions within the p97/VCP pore.

D2 Arginine Denaturation Collar

The nature of the residues in the D2 domain discussed above invites speculation on how p97/VCP interacts with its substrates. Arginine would be an ideal residue to promote protein unfolding: its functional end resembles guanidine, a protein denaturant presumed to function by stabilizing the unfolded protein state (Greene and Pace, 1974; Mason et al., 2003). The arrangement of Arg586 and Arg599 within the hexamer is such that the 12 guanidyl groups of the Arg586/Arg599 residues are located within a volume (~1700 Å^3) that could accommodate ~50 water molecules. Assuming that the functional group of arginine is at least equivalent to two-thirds of a guanidine molecule, the coincidence of the 12 guanidyl groups within the D2 pore is theoretically equivalent to an 8 M solution of guanidine, a concentration sufficient to denature most proteins. The double ring structure of Arg586/Arg599 could thus be thought of as a "denaturation collar" (Figure 1A, panel I), able to dissolve secondary structure in preparation for subsequent substrate processing events. Moreover, the functionally important residues Phe551 and Trp552 immediately beneath the denaturation collar interact with the substrate. Putative denaturation by the Arg586/Arg599 collar coupled with the large conformational change of the Phe551/Trp552 region observed during the ATP hydrolysis cycle may provide a driving force to engage and dislocate proteins from the ER.

Substrate Does Not Pass through the D1 Pore

In the D1 domain, we focused our attention on a loop that lines the narrowest region in the central pore. Our crystal structures have shown that this region is a relatively static part of the molecule (DeLaBarre and Brunger, 2003, 2005). Barring unobserved conformational changes, a dislocating substrate passing through the pore at the D1 end would necessarily make contact with the conserved residues comprising this loop (Figure 1B, panel III). Only His317 showed significant effects on ERAD, while mutations at neighboring residues in the D1 pore (Arg313, Lys315, Thr316, Glu319) showed no effect (Figure 2D). The observation that only one D1 pore residue significantly impacted ERAD suggests that dislocating substrate does not pass through D1's narrow pore. To understand why only His317 is important for p97/VCP's function in ERAD, we must consider both its location in the structure and the effect of the p97/VCP^{H317A} mutant upon ATP hydrolysis (Figures 2A–2C). His317 is more than 20 Å from the nucleotide binding site, so it is unlikely to play a direct role in ATP hydrolysis. However, the p97/VCP^{H317A} mutant exhibited a dramatic switch from positive to anticooperative behavior (Figure 2B). ATP-trapping experiments (Zalk and Shoshan-Barmatz, 2003), as well as the Hill coefficient measured here and by others (Song et al., 2003) for p97/VCP^{wt}, indicate that two protomers are acting together during ATP hydrolysis. When we consider that His317 is the closest common point of contact for all six protomers (Figure 1B, panel III), these combined results suggest a model whereby His317 serves as an interaction nexus for the six protomers. Disrupting this interaction is likely to affect the function of the p97/VCP hexamer and, in turn, impair its function within ERAD.

A Model for Protein Dislocation by p97/VCP

Our results suggest a model for protein dislocation whereby substrate interacts primarily with the D2 end of p97/VCP and does not pass through the D1 domain. In our model, the D1 domain is primarily responsible for maintaining the integrity of the intraprotomer interactions. In light of known protein-protein interactions (Lilley and Ploegh, 2004; Ye et al., 2001, 2004), detailed observations of conformational changes (DeLaBarre and Brunger, 2005), and the results of this study, we propose a model whereby dislocating substrate enters into the pore created by the D2 domains. The exact relationship between p97/VCP, adaptor proteins, and substrate is currently unknown. Interactions between the N domains of p97/VCP and adaptor proteins like Ufd1/Npl4 do not preclude the binding of additional cofactors with other regions of p97/VCP, such as the D2 domain. In fact, the recently identified accessory proteins (Ufd2, Ufd3, and Otu1) that bind the ATPase domains of Cdc48p (Rumpf and Jentsch, 2006) may help to guide substrates beyond their initial engagement with the D2 domain. The conformational state of dislocating substrates is also not yet fully understood, but such a process could be facilitated by the disruption of substrate structure by the denaturation collar. Substrate may either exit back out through the main D2 pore opening or through transient openings near the D1/D2 interface, or simply become sufficiently segregated inside p97/VCP for removal from the ER when p97/VCP dissociates from the membrane.

Experimental Procedures

Protein Expression

Point mutants of p97/VCP were created using the Stratagene QuikChange protocol and verified by sequencing. Myc-tagged p97/VCP constructs used for mammalian expression were subcloned into the pMACS4-IRES II vector (Miltenyi Biotec). TCRα-GFP was constructed by fusing the 2B4 isoform of mouse TCRα to EGFP using standard PCR techniques and was cloned into the pcDNA3.1(+) expression vector (Invitrogen). The shRNA sequence targeting p97/VCP has been described previously (Wojcik et al., 2004). The p97/VCP shRNA was expressed in the plasmid pSUPERSTAR, a derivative of the pG-SUPER vector (Kojima et al., 2004) in which GFP has been replaced with ΔCD4. Empty pSUPERSTAR vector was used as a control for expression.

Full-length rat SytI was amended with C-terminal hemagglutinin tag (SytI-HA) and subcloned into pcDNA3 (Invitrogen). All

mammalian expression plasmids were transfected with Fugene-6 (Roche) and assays performed 60 hr posttransfection.

p97/VCP^{wt} and mutant proteins were expressed in *E. coli* and purified as described previously (DeLaBarre and Brunger, 2003). The cytoplasmic domain of SytI, residues 96–421, with the single-site mutation C273S, was purified as previously described (Bowen et al., 2005; Ernst and Brunger, 2003).

Cell-Based Assay

TCRα-GFP expressing HEK293 clonal cell lines were selected for low basal GFP levels and robust responses to the MG132 (10 μM, 12 hr) and used for all experiments described. SytI-HA was transiently expressed in HEK293 cells. All cells were maintained in Dulbecco's modified Eagle's medium + 10% fetal bovine serum (FBS) at 37ºC and 5% CO_2.

Two-color analysis of transfected reporter cells employed anti-CD4-allophycocyanin (CD4-APC, Caltag) and was performed on a FACSCalibur flow cytometer (Becton Dickinson). Gates were set to measure GFP fluorescence in three sets of 10,000 CD4$^+$ cells and the mean GFP fluorescence determined for each. Values were normalized to the mean fluorescence measured from cells expressing p97/VCP^{wt}. Average and standard deviation for each mutant were calculated from normalized values (n = 3).

Immunoprecipitation, Western blot, and immunofluorescence analyses were performed with the following: polyclonal (kind gift of M. Rexach) and monoclonal (Roche) anti-GFP, monoclonal anti-ubiquitin (Chemicon), anti-myc (9E10 clone), polyclonal anti-p97/VCP (gift of C.C. Li), and anti-HA (12CA5).

Reporter cells transfected with p97/VCP-myc constructs were lysed in 1% Triton X-100 lysis buffer (Christianson and Green, 2004). Lysates were loaded onto 10%–30% continuous sucrose gradients and centrifuged in a Beckman SW 41 rotor for 16 hr at 39,000 rpm at 4ºC. Five hundred microliter samples were collected from the top of the gradient, and protein was precipitated by trichloroacetic acid. Samples were resolubilized in SDS-sample buffer and run on 7.5% SDS-PAGE gels.

Steady-State Kinetics

Steady-state kinetics parameters were determined by continual colorimetric monitoring of phosphate release during p97/VCP-catalyzed ATP hydrolysis. Phosphate release from p97/VCP was measured by monitoring the phosphate-dependent cleavage of 2-amino-6-mercapto-7methyl guanoside (MESG) (Webb, 1992). The cleavage of MESG results in an absorption shift from 330 to 360 nm. Reactions were carried out in 96-well plates, and the absorption at 360 nm was continually monitored with a SpectraMax Plus^{384} plate reader (Molecular Devices, Sunnyvale, California) at 37ºC. The total reaction volume was 300 μl and buffered with 25 mM Tris-HCl (pH 7.5) and 10 mM $MgCl_2$ (buffer A). Concentration studies (data not shown) showed that 10 mM $MgCl_2$ produced optimum ATPase activity for p97/VCP^{wt}. Purified protein was exchanged into buffer A and quantified by a Bradford assay. Total protein content ranged from 15 to 50 μg and was adjusted for individual mutants to give linear results for the complete ATP concentration range for at least the first 200 s of the reaction. Reactions were initiated by addition of 50 μl of ATP solution after preincubating all solutions at 37ºC. Rates were measured by taking the slope of the signal in the linear portion of the reaction, typically between 20 and 200 s, and then subtracting background values. Background values were established by performing the reactions with protein in the absence of ATP. In the absence of protein, ATP at the concentrations used in these experiments did not produce a signal above background. p97/VCP^{wt} protein concentrations were chosen to produce the most dynamic range for the progress curves (Figure S2). p97/VCP mutant protein concentrations were chosen at the same concentration as p97/VCP^{wt} when possible. For mutants that exhibited a strong decrease in k_{cat}, the protein concentration was increased to obtain a measurable signal. The ATP concentrations used for progress curves of individual mutants were optimized according to individual kinetic parameters. In all cases, the [ATP]:[p97/VCP] ratio was at least 500 to satisfy the criteria for Michaelis-Menten kinetic analysis. The steady-state constants V_{max}, K_M, and n were obtained by fitting the progress curves to the Hill equation, $\nu = (V_{max}[S])^n / (K_M{}^n + [S]^n)$ (Neet, 1996), using Origin 7.0 (OriginLab). k_{cat} was calculated from the observed V_{max} and the amount of protein added to reaction mix, as determined by the Bradford method. Error estimates associated with the fitted values were determined by the nonlinear fitting procedure. Reactions were done in duplicate for any single progressive curve, and a minimum of two independent experiments was carried out for both the mutants and wild-type. The errors derived from the variation of these repeated experiments were similar to the estimated errors of the individual fits.

Two hundred picomoles of the cytoplasmic fragment of SytI was added to varying amounts of VCP/p97. Five picomoles of p97/VCP^{wt} (based on hexamer molecular weight) was used. The increase in wild-type activity could be observed with [SytI]:[VCP/p97$_6$] ratios as low as 4:1, and an effect in the native gel could be seen at a 2.5:1 molar ratio (Figure 3B). The amount of mutant protein was adjusted to give measurable signals in the assays but did not exceed 50 pmol. The ATP concentration was 215 μM, a saturating amount for both p97/VCP^{wt} and mutants. The p97/VCP · SytI mixture was incubated for 2 min at 37ºC before ATP was added to initiate the reaction. The reaction was carried out as described above. SytI had no effect upon the reporter assay, as determined by calibration with phosphate standards. Reactions ±SytI were done in duplicate for any single progressive curve, and a minimum of three independent experiments was carried out for both the mutants and wild-type. The increase in ATPase activity was calculated by taking the ratio of the reaction with synaptotagmin to the reaction without synaptotagmin for the wild-type and each of the mutants.

Mass Spectrometry

We followed a previously developed protocol using isotope mixtures of crosslinker to identify crosslinked fragments (Sinz, 2003). The method creates a characteristic M, M+4 pattern for crosslinked fragments. Briefly, 1.5 nmol of VCP/p97 hexamer was mixed with 27 nmol of the cytoplasmic fragment of SytI in a 1 ml solution of 20 mM HEPES (pH 7.3). A solution of a 1:1 mixture of bis(Sulfosuccinimidyl)glutarate (BS^2) and its deuterated analog (BS^2-D4) (Pierce Chemical) in dimethylsulfoxide was added to the protein solution to a final concentration of 6 mM. The reaction was incubated for 1 hr at ambient temperature. A faint band just past the 117 kDa marker, corresponding with a 1:1 complex between p97/VCP monomer and SytI, was observed in a Coomassie-stained SDS-PAGE gel of the reaction. Higher molecular weight bands were observed, but they were also visible when proteins were individually crosslinked under similar conditions.

The gel was destained, and the band was excised, crushed, washed in 25 mM ammonium bicarbonate/50% acetonitrile, dried, reduced, derivatized with iodoacetamide, and digested with trypsin as described (Jiménez et al., 1998). Recovered peptides were adsorbed onto uC18 ZipTips (Millipore, Bedford, Massachusetts), washed with 0.1% TFA, then eluted with 3–4 μl of 50% acetonitrile/50% water with 0.1% TFA.

The tryptic peptide mixture from the gel band was combined with an equal volume of matrix solution and allowed to dry on the MALDI target. The matrix solution used was a 10 g/L solution of α-cyano-4-hydroxycinnamic acid in 50% acetonitrile/50% water with 0.1% TFA. All mass spectrometric measurements were performed on an Applied Biosystems (Foster City, California) 4700 Proteomics Analyzer, which is a tandem time-of-flight instrument (TOF/TOF) with a MALDI ion source (Bienvenut et al., 2002). Reflector spectra were acquired to determine the masses of the peptides of interest. Normal tryptic fragments of the starting proteins were used to calibrate the mass scale. Peaks of the reflector spectra were filtered by the requirement that crosslinked species have to occur in pairs 4 atomic mass units apart, corresponding to the two isotopes of the crosslinker.

Peaks were observed at 2294.10 and 2298.18 m/z (monoisotopic protonated molecular weight, MH$^+$), which correspond to a crosslinked fragment of residues 561–567 (E I F D K A R) in p97/VCP and residues 234–244 (F S K H D I I G E F K) in SytI. The observed and the calculated masses differ by ~35 ppm: 877.47 + 1319.69 + 96.01 (crosslinker) + 1.01 (observing MH^{+1} species) = 2294.18, versus 2294.10 observed.

Supplemental Data

Supplemental Data include five figures and can be found with this article online at www.molecule.org/cgi/content/full/22/4/451/DC1/.

Acknowledgments

We thank D. King and A. Falick, HHMI mass spectrometry lab at the University of California at Berkeley, for carrying out the mass spectrometry experiments; E. Bennett, A. McClellan, and T. Fenn for discussions; and CFRI (J.C.C.) and NIDDK (R.R.K.) for grant support.

Received: January 27, 2006
Revised: March 6, 2006
Accepted: March 31, 2006
Published: May 18, 2006

References

Beuron, F., Flynn, T.C., Ma, J., Kondo, H., Zhang, X., and Freemont, P.S. (2003). Motions and negative cooperativity between p97 domains revealed by cryo-electron microscopy and quantised elastic deformational model. J. Mol. Biol. *327*, 619–629.

Beyer, A. (1997). Sequence analysis of the AAA protein family. Protein Sci. *6*, 2043–2058.

Bienvenut, W.V., Deon, C., Pasquarello, C., Campbell, J.M., Sanchez, J.C., Vestal, M.L., and Hochstrasser, D.F. (2002). Matrix-assisted laser desorption/ionization-tandem mass spectrometry with high resolution and sensitivity for identification and characterization of proteins. Proteomics *2*, 868–876.

Bowen, M.E., Weninger, K., Ernst, J., Chu, S., and Brunger, A.T. (2005). Single-molecule studies of synaptotagmin and complexin binding to the SNARE complex. Biophys. J. *89*, 690–702.

Christianson, J.C., and Green, W.N. (2004). Regulation of nicotinic receptor expression by the ubiquitin-proteasome system. EMBO J. *23*, 4156–4165.

Dalal, S., Rosser, M.F., Cyr, D.M., and Hanson, P.I. (2004). Distinct roles for the AAA ATPases NSF and p97 in the secretory pathway. Mol. Biol. Cell *15*, 637–648.

Davies, J.M., Tsuruta, H., May, A.P., and Weis, W.I. (2005). Conformational changes of p97 during nucleotide hydrolysis determined by small-angle X-ray scattering. Structure (Camb) *13*, 183–195.

DeLaBarre, B., and Brunger, A.T. (2003). Complete structure of p97/valosin-containing protein reveals communication between nucleotide domains. Nat. Struct. Biol. *10*, 856–863.

DeLaBarre, B., and Brunger, A.T. (2005). Nucleotide dependent motion and mechanism of action of p97/VCP. J. Mol. Biol. *347*, 437–452.

Ernst, J.A., and Brunger, A.T. (2003). High resolution structure, stability, and synaptotagmin binding of a truncated neuronal SNARE complex. J. Biol. Chem. *278*, 8630–8636.

Feiler, H.S., Desprez, T., Santoni, V., Kronenberger, J., Caboche, M., and Traas, J. (1995). The higher plant Arabidopsis thaliana encodes a functional CDC48 homologue which is highly expressed in dividing and expanding cells. EMBO J. *14*, 5626–5637.

Fiebiger, E., Hirsch, C., Vyas, J.M., Gordon, E., Ploegh, H.L., and Tortorella, D. (2004). Dissection of the dislocation pathway for type I membrane proteins with a new small molecule inhibitor, eeyarestatin. Mol. Biol. Cell *15*, 1635–1646.

Frohlich, K.U., Fries, H.W., Rudiger, M., Erdmann, R., Botstein, D., and Mecke, D. (1991). Yeast cell cycle protein CDC48p shows full-length homology to the mammalian protein VCP and is a member of a protein family involved in secretion, peroxisome formation, and gene expression. J. Cell Biol. *114*, 443–453.

Greene, R.F., Jr., and Pace, C.N. (1974). Urea and guanidine hydrochloride denaturation of ribonuclease, lysozyme, alpha-chymotrypsin, and beta-lactoglobulin. J. Biol. Chem. *249*, 5388–5393.

Han, W., Rhee, J.S., Maximov, A., Lao, Y., Mashimo, T., Rosenmund, C., and Südhof, T.C. (2004). N-glycosylation is essential for vesicular targeting of synaptotagmin 1. Neuron *41*, 85–99.

Hinnerwisch, J., Reid, B.G., Fenton, W.A., and Horwich, A.L. (2005). Roles of the N-domains of the ClpA unfoldase in binding substrate proteins and in stable complex formation with the ClpP protease. J. Biol. Chem. *280*, 40838–40844.

Huppa, J.B., and Ploegh, H.L. (1997). The alpha chain of the T cell antigen receptor is degraded in the cytosol. Immunity *7*, 113–122.

Huyton, T., Pye, V.E., Briggs, L.C., Flynn, T.C., Beuron, F., Kondo, H., Ma, J., Zhang, X., and Freemont, P.S. (2003). The crystal structure of murine p97/VCP at 3.6Å. J. Struct. Biol. *144*, 337–348.

Jarosch, E., Taxis, C., Volkwein, C., Bordallo, J., Finley, D., Wolf, D.H., and Sommer, T. (2002). Protein dislocation from the ER requires polyubiquitination and the AAA-ATPase Cdc48. Nat. Cell Biol. *4*, 134–139.

Jiménez, C.R., Huang, L., Qiu, Y., and Burlingame, A.L. (1998). In-gel digestion of proteins for MALDI-MS fingerprint mapping. In Current Protocols in Protein Science, V.B. Chanda, ed. (New York: John Wiley & Sons), pp. 16.4.1–16.4.5.

Kojima, S., Vignjevic, D., and Borisy, G.G. (2004). Improved silencing vector co-expressing GFP and small hairpin RNA. Biotechniques *36*, 74–79.

Kopito, R.R. (1997). ER quality control: the cytoplasmic connection. Cell *88*, 427–430.

Kozutsumi, Y., Segal, M., Normington, K., Gething, M.J., and Sambrook, J. (1988). The presence of malfolded proteins in the endoplasmic reticulum signals the induction of glucose-regulated proteins. Nature *332*, 462–464.

Lamb, J.R., Fu, V., Wirtz, E., and Bangs, J.D. (2001). Functional analysis of the trypanosomal AAA protein TbVCP with trans-dominant ATP hydrolysis mutants. J. Biol. Chem. *276*, 21512–21520.

Lee, R.J., Liu, C.W., Harty, C., McCracken, A.A., Latterich, M., Romisch, K., DeMartino, G.N., Thomas, P.J., and Brodsky, J.L. (2004). Uncoupling retro-translocation and degradation in the ER-associated degradation of a soluble protein. EMBO J. *23*, 2206–2215.

Lilley, B.N., and Ploegh, H.L. (2004). A membrane protein required for dislocation of misfolded proteins from the ER. Nature *429*, 834–840.

Lum, R., Tkach, J.M., Vierling, E., and Glover, J.R. (2004). Evidence for an unfolding/threading mechanism for protein disaggregation by Saccharomyces cerevisiae Hsp104. J. Biol. Chem. *279*, 29139–29146.

Lupas, A.N., and Martin, J. (2002). AAA proteins. Curr. Opin. Struct. Biol. *12*, 746–753.

Mason, P.E., Neilson, G.W., Dempsey, C.E., Barnes, A.C., and Cruickshank, J.M. (2003). The hydration structure of guanidinium and thiocyanate ions: implications for protein stability in aqueous solution. Proc. Natl. Acad. Sci. USA *100*, 4557–4561.

Meyer, H.H., Kondo, H., and Warren, G. (1998). The p47 co-factor regulates the ATPase activity of the membrane fusion protein, p97. FEBS Lett. *437*, 255–257.

Meyer, H.H., Shorter, J.G., Seemann, J., Pappin, D., and Warren, G. (2000). A complex of mammalian ufd1 and npl4 links the AAA-ATPase, p97, to ubiquitin and nuclear transport pathways. EMBO J. *19*, 2181–2192.

Miller, K.G. (1993). The proteins of synaptic vesicles: descriptive and functional studies. PhD thesis, Stanford University, Stanford, California.

Neet, K.E. (1996). Cooperativity in enzyme function: equilibrium and kinetic aspects. In Contemporary Enzyme Kinetics and Mechanism, D.L. Purich, ed. (San Diego: Academic Press), pp. 133–182.

Neuwald, A.F., Aravind, L., Spouge, J.L., and Koonin, E.V. (1999). AAA^{+}: a class of chaperone-like ATPases associated with the assembly, operation, and disassembly of protein complexes. Genome Res. *9*, 27–43.

Ogura, T., Whiteheart, S.W., and Wilkinson, A.J. (2004). Conserved arginine residues implicated in ATP hydrolysis, nucleotide-sensing, and inter-subunit interactions in AAA and AAA(+) ATPases. J. Struct. Biol. *146*, 106–112.

Pinter, M., Jekely, G., Szepesi, R.J., Farkas, A., Theopold, U., Meyer, H.E., Lindholm, D., Nassel, D.R., Hultmark, D., and Friedrich, P. (1998). TER94, a Drosophila homolog of the membrane fusion protein CDC48/p97, is accumulated in nonproliferating cells: in the reproductive organs and in the brain of the imago. Insect Biochem. Mol. Biol. *28*, 91–98.

Rabinovich, E., Kerem, A., Frohlich, K.U., Diamant, N., and Bar-Nun, S. (2002). AAA-ATPase p97/Cdc48p, a cytosolic chaperone required

for endoplasmic reticulum-associated protein degradation. Mol. Cell. Biol. *22*, 626–634.

Roggy, J.L., and Bangs, J.D. (1999). Molecular cloning and biochemical characterization of a VCP homolog in African trypanosomes. Mol. Biochem. Parasitol. *98*, 1–15.

Rumpf, S., and Jentsch, S. (2006). Functional division of substrate processing cofactors of the ubiquitin-selective Cdc48 chaperone. Mol. Cell *21*, 261–269.

Sinz, A. (2003). Chemical cross-linking and mass spectrometry for mapping three-dimensional structures of proteins and protein complexes. J. Mass Spectrom. *38*, 1225–1237.

Song, C., Wang, Q., and Li, C.C. (2003). ATPase activity of p97-valosin-containing protein (VCP): D2 mediates the major enzyme activity, and D1 contributes to the heat-induced activity. J. Biol. Chem. *278*, 3648–3655.

Sousa, M.C., Trame, C.B., Tsuruta, H., Wilbanks, S.M., Reddy, V.S., and McKay, D.B. (2000). Crystal and solution structures of an HslUV protease-chaperone complex. Cell *103*, 633–643.

Sugita, S., and Südhof, T.C. (2000). Specificity of Ca^{2+}-dependent protein interactions mediated by the C_2A domains of synaptotagmins. Biochemistry *39*, 2940–2949.

Sutton, R.B., Davletov, B.A., Berghuis, A.M., Südhof, T.C., and Sprang, S.R. (1995). Structure of the first C_2 domain of synaptotagmin I: a novel Ca^{2+}/phospholipid-binding fold. Cell *80*, 929–938.

Tiwari, S., and Weissman, A.M. (2001). Endoplasmic reticulum (ER)-associated degradation of T cell receptor subunits: involvement of ER-associated ubiquitin-conjugating enzymes (E2s). J. Biol. Chem. *276*, 16193–16200.

Wang, Q., Song, C., and Li, C.C. (2003). Hexamerization of p97-VCP is promoted by ATP binding to the D1 domain and required for ATPase and biological activities. Biochem. Biophys. Res. Commun. *300*, 253–260.

Webb, M.R. (1992). A continuous spectrophotometric assay for inorganic phosphate and for measuring phosphate release kinetics in biological systems. Proc. Natl. Acad. Sci. USA *89*, 4884–4887.

Weibezahn, J., Tessarz, P., Schlieker, C., Zahn, R., Maglica, Z., Lee, S., Zentgraf, H., Weber-Ban, E.U., Dougan, D.A., Tsai, F.T., et al. (2004). Thermotolerance requires refolding of aggregated proteins by substrate translocation through the central pore of ClpB. Cell *119*, 653–665.

Wojcik, C., Yano, M., and DeMartino, G.N. (2004). RNA interference of valosin-containing protein (VCP/p97) reveals multiple cellular roles linked to ubiquitin/proteasome-dependent proteolysis. J. Cell Sci. *117*, 281–292.

Ye, Y., Meyer, H.H., and Rapoport, T.A. (2001). The AAA ATPase Cdc48/p97 and its partners transport proteins from the ER into the cytosol. Nature *414*, 652–656.

Ye, Y.H., Shibata, Y., Yun, C., Ron, D., and Rapoport, T.A. (2004). A membrane protein complex mediates retro-translocation from the ER lumen into the cytosol. Nature *429*, 841–847.

Yu, H., and Kopito, R.R. (1999). The role of multiubiquitination in dislocation and degradation of the alpha subunit of the T cell antigen receptor. J. Biol. Chem. *274*, 36852–36858.

Yu, H., Kaung, G., Kobayashi, S., and Kopito, R.R. (1997). Cytosolic degradation of T-cell receptor alpha chains by the proteasome. J. Biol. Chem. *272*, 20800–20804.

Zalk, R., and Shoshan-Barmatz, V. (2003). ATP-binding sites in brain p97/VCP (valosin-containing protein), a multifunctional AAA ATPase. Biochem. J. *374*, 473–480.

Zhong, X., Shen, Y., Ballar, P., Apostolou, A., Agami, R., and Fang, S. (2004). AAA ATPase p97/valosin-containing protein interacts with gp78, a ubiquitin ligase for endoplasmic reticulum-associated degradation. J. Biol. Chem. *279*, 45676–45684.